

Enhancing Speckle Statistics for Imaging Inside Scattering Media

WEI-YU CHEN¹, MATTHEW O'TOOLE¹, ASWIN C. SANKARANARAYANAN¹, AND ANAT LEVIN^{2,*}

¹Carnegie Mellon University, 5000 Forbes Avenue Pittsburgh, PA 15213

²Technion, Israel, Technion City, Haifa 3200003, Israel

*Corresponding author: weiyuc@andrew.cmu.edu

Compiled October 31, 2022

We exploit memory effect correlations in speckles for the imaging of incoherent fluorescent sources behind scattering tissue. These correlations are often weak when imaging thick scattering tissues and complex illumination patterns, both of which greatly limit the practicality of associated techniques. In this work, we introduce a spatial light modulator between the tissue sample and the imaging sensor and capture multiple modulations of the speckle pattern. We show that, by correctly designing the modulation patterns and the associated reconstruction algorithm, the statistical correlations in the measurements can be greatly enhanced. We exploit this to demonstrate the reconstruction of mega-pixel sized fluorescent patterns behind the scattering tissue. © 2022 Optica Publishing Group

<http://dx.doi.org/10.1364/ao.XX.XXXXXX>

1. INTRODUCTION

Scattering of light is one of the main barriers preventing the imaging of fluorescent sources located deep inside biological tissue. A microscope imaging a set of incoherent sources inside the tissue usually observes a noisy speckle pattern that has little resemblance to the actual sources.

Despite the noise-like appearance, speckle has strong statistical properties, such as the *memory effect* (ME), implying that the patterns generated by nearby sources are correlated. It has been previously observed that due to this ME correlation, the auto-correlation of a speckle pattern generated by multiple independent sources is equivalent to the auto-correlation of the latent source layout [1–10]. This fascinating property has drawn a lot of interest since it allows the recovery of latent illuminators, completely invisible to the naked eye, purely by exploiting speckle statistics.

Despite its potential, there are still major challenges to solve before the idea can apply to realistic biomedical imaging scenarios. The main barrier is that ME correlations are very weak and the amount of information that can be inferred from them is limited. To circumvent this, past experimental demonstrations have made use of various simplifying assumptions. While fluorescent sources of interest in realistic biomedical imaging scenarios are located inside the scattering sample rather than far behind it, most demonstrations of speckle correlation-based see-through algorithms consider sources located a few centimeters beyond the sample. This is due to the fact that when the sources are further from the scattering layer [11], they span a smaller range of angles relative to the layer and therefore speckle cor-

relations are stronger. A second issue is that the contrast of the observed speckle pattern decays as more independent emitters are present, and hence, the technique is mostly applicable to very sparse emitter layouts.

In this work, we exploit strategies for maximizing the amount of ME correlation we can extract from speckle images. To this end, we build on a simple observation: if we could image the same layout of fluorescent sources through different scattering layers, we could obtain multiple independent speckle images of the same target, leading to independent auto-correlations. Averaging such independent auto-correlations can suppress noise in the correlations and boost the quality of the illuminator patterns that we can infer from it. While some temporal dynamics are present in live tissue, sequential images of illuminators inside the same tissue are still highly correlated. Rather, we use a programmable spatial light modulator (SLM) mask in the optical path imaging the tissue and use it to modulate the field, leading to different speckle images. We discuss various forms of speckle diversification and arrive at a spatial form of modulation based on lateral shearing interferometry (LSI). We show that despite the fact that we image the same tissue layer multiple times, we can get uncorrelated measurements that maximize ME correlation.

To further maximize the amount of information that we can extract from speckle data, we follow an idea recently proposed by [11], which argues that when light sources are located inside the sample rather than far behind it, the speckle pattern generated by each source has a limited support and does not spread over the full sensor. Thus, rather than computing a global full-frame auto-correlation, they compute local auto-correlations

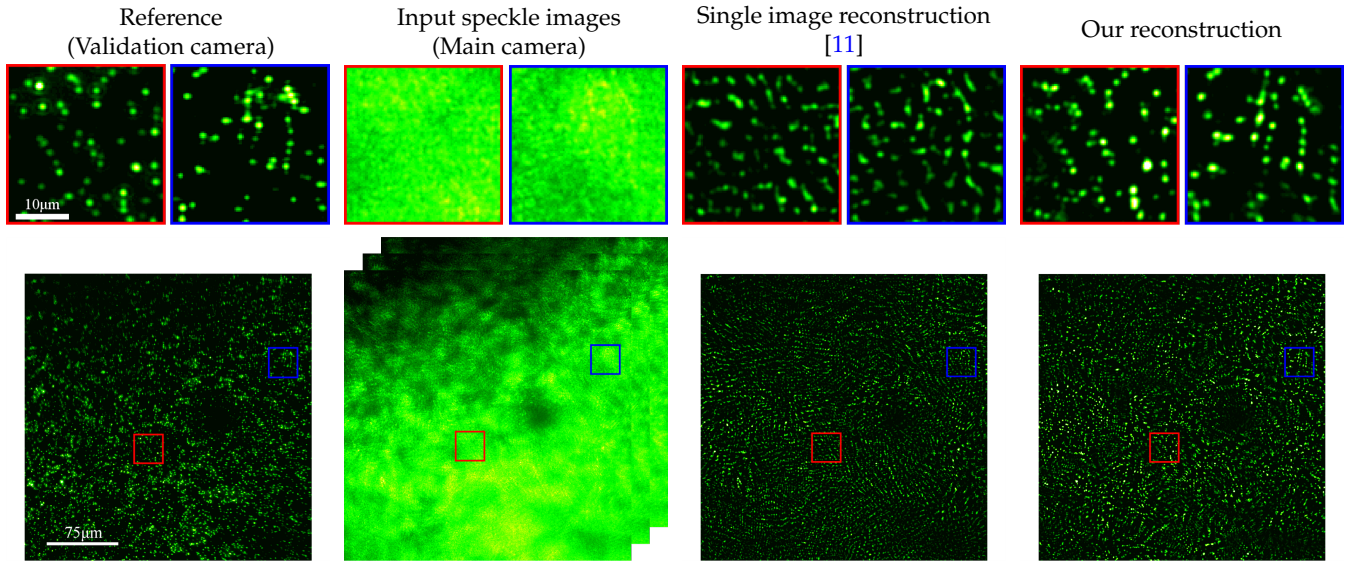


Fig. 1. Reconstructing a wide-range fluorescent bead target from modulated speckles. We reconstruct the layout of fluorescent beads spread behind a chicken breast tissue slice, whose thickness was measured at about $\sim 150\mu\text{m}$. The beads are attached to the tissue, separated only by a $150\mu\text{m}$ cover glass. The beads spread over a field of view of $300\mu\text{m} \times 300\mu\text{m}$, occupying a one mega pixel image. While the ME correlations in a single image capture are too noisy to provide good reconstruction, we optically modulate the speckle field, capturing 54 shots with different modulations. This modulation allows us to amplify statistical correlations, leading to accurate reconstruction of a complex illuminator pattern, despite high degradation and limited speckle contrast in the input images. The lower part of the figure includes the full images, while at the top we zoom on two sub windows for high resolution visualization.

in the form of a Ptychography algorithm [12–16]. These local correlations can boost the signal to noise ratio of the detected correlation by a few orders of magnitude.

Combining our speckle diversification with the local correlations of [11], we demonstrate the reconstruction of wide, complex fluorescent bead patterns inside scattering tissue. Our approach captures only a few dozen images of the tissue, compared to hundreds of images used by recent approaches that image fluorescent sources behind scattering layers [17, 18] when using single-photon fluorescent emission. Compared to recent wavefront shaping approaches [19, 20] that only facilitate imaging of a local neighborhood governed by the limited extent of the ME, our approach recovers mega-pixel images over a wide field of view, as demonstrated in Fig. 1.

2. PRINCIPLE

A. A review of ME-based imaging

We start with a quick review of the ME and its application for seeing inside scattering media. Let $\mathbf{i}^1, \mathbf{i}^2$ denote the position of two illumination sources and $u^{\mathbf{i}^1}(\mathbf{v}), u^{\mathbf{i}^2}(\mathbf{v})$ the fields they generate, where \mathbf{v} denotes a sensor coordinate. The ME states that speckle fields generated by *nearby* sources are related by a tilt-shift correlation [21]. Recently, Bar *et al.* [22] have offered a simple model for this relation, stating that

$$u^{\mathbf{i}^1}(\mathbf{v}) \approx e^{ik\alpha(\Delta^T \tau)} u^{\mathbf{i}^2}(\mathbf{v} + \Delta), \quad (1)$$

with $\Delta = \mathbf{i}^2 - \mathbf{i}^1$ the displacement between the sources, $\tau = \mathbf{v} - \mathbf{i}^1$ the displacement between the source to the observation point, and $\alpha \approx \frac{3}{2L}$, where L is the tissue thickness. This model assumes that we image the volume with a microscope whose sensor plane is conjugate to the plane of the illuminators $\mathbf{i}^1, \mathbf{i}^2$.

An image sensor only measures the intensity of the speckle pattern which we denote by

$$S^{\mathbf{i}^n}(\mathbf{v}) = |u^{\mathbf{i}^n}(\mathbf{v})|^2. \quad (2)$$

In the presence of multiple incoherent illuminators, we observe an intensity image $I(\mathbf{v}) = \sum_n S^{\mathbf{i}^n}(\mathbf{v}) = \sum_n |u^{\mathbf{i}^n}(\mathbf{v})|^2$. Assuming source displacements are small enough for ME correlation to hold, speckle intensities from nearby sources are shifted versions of each other, $S^{\mathbf{i}^1}(\mathbf{v}) \approx S^{\mathbf{i}^2}(\mathbf{v} + \Delta)$. Note that since we deal with intensity images, phase adjustments are not required.

We denote by $S^0(\mathbf{v})$ the speckle from an illumination source at the center of the frame. With this notation, we can express the sum of speckles from incoherent sources as

$$I = S^0(\mathbf{v}) * O, \quad (3)$$

where O is a binary image denoting the location of the illumination sources, and $*$ denotes convolution. To detect fluorescent sources through scattering media, our goal is to recover the latent illuminator pattern O from an input speckle image I .

We now filter I and S^0 to locally have a zero mean

$$\bar{I} = I - g * I, \quad \bar{S}^0 = S^0 - g * S^0, \quad (4)$$

where g is a low pass filter. We note that Eq. (3) also holds if we replace I, S^0 with \bar{I}, \bar{S}^0 , and we can express $\bar{I} = \bar{S}^0 * O$. Since \bar{S}^0 is a random zero mean signal, its auto-correlation is approximately an impulse function [2]

$$\bar{S}^0 * \bar{S}^0 \approx \delta. \quad (5)$$

With this approximation prior work [1, 2] derive the relationship:

$$\bar{I} * \bar{I} = (\bar{S}^0 * \bar{S}^0) * (O * O) \approx O * O, \quad (6)$$

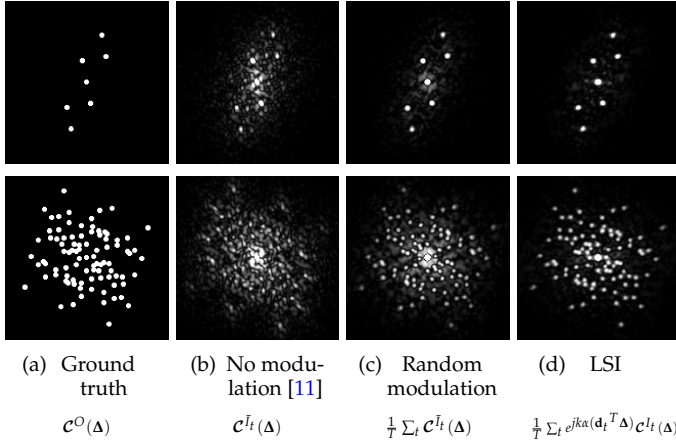


Fig. 2. Comparing speckle auto-correlation with different modulation approaches. The two rows compare illuminator layouts with different complexities, while the columns evaluate different diversification strategies. All results use the same number of shot images captured with the setup of Fig. 5. The illuminator layout of the second row is shown in the first row of Fig. 6. (a) Ground truth auto-correlation. (b) Without any modulation, reconstructed auto-correlation is noisy, and when the target is complex (2nd row), it is almost unrecognizable. (c) Random modulation can improve contrast, but still contains noise. (d) LSI can clearly recover the auto-correlation.

where \star denotes cross correlation. Thus, the auto-correlation of the input speckle intensity is equivalent to the auto-correlation of the desired latent image O . As a result, one can recover O from $\bar{I} \star \bar{I}$ using a phase retrieval algorithm [2].

Challenges. The observation made by Eq. (6) is very compelling because it suggests that latent illuminators O can be recovered from a noisy speckle image I , despite the fact that to the untrained eye, the input images carry no similarity to the latent source layout. Yet, it involves two major assumptions that limit its practical applicability.

The first problem is that the ME correlation is not exact, especially when the displacement between the illuminators increase. A second problem is that since the speckle pattern S^0 emerging from a single source has a limited support and only spans a finite number of pixels, its auto-correlation $S^0 \star S^0$ outlined in Eq. (5) is not a perfect impulse, but involves residual noise. Supplementary Fig. S3 illustrates this difference. Effectively, in realistic scenarios, $\bar{I} \star \bar{I}$ is a *very* noisy approximation to $O \star O$. This noise increases as more independent illuminators are present in O .

In Fig. 2(b), we show the auto-correlation of a speckle image \bar{I} composed of a sparse layout of sources. We compare two layouts with a different number of sources. We can see that as more incoherent sources are included, the auto-correlation is very noisy and does not resemble $O \star O$. Our goal in this work is to improve the contrast of this auto-correlation by capturing multiple diversified speckle signals.

B. Improving auto-correlation contrast

To analyze the contrast of the speckle correlation, we introduce the following notation. We denote by Γ_Δ the set of all displacements Δ , such that our latent pattern includes a pair of illuminators (n, m) displaced by Δ :

$$\Gamma_\Delta = \{\Delta | \exists(n, m), \Delta = \mathbf{i}^m - \mathbf{i}^n\}, \quad (7)$$

and by Γ_Δ^c the list of all other displacements. We denote the speckle auto-correlation by \mathcal{C}^I , which is defined for a displacement Δ as:

$$\mathcal{C}^I(\Delta) = \sum_{\mathbf{v}} \bar{I}(\mathbf{v}) \bar{I}(\mathbf{v} + \Delta). \quad (8)$$

Intuitively, the speckle correlation has good contrast if $\mathcal{C}^I(\Delta)$ is high for displacements $\Delta \in \Gamma_\Delta$, corresponding to real illuminator positions; and is low for all other displacements $\Delta \in \Gamma_\Delta^c$. We define the correlation contrast using the following signal to noise metric:

$$\Theta(\mathcal{C}^I) = \frac{\frac{1}{|\Gamma_\Delta|} \sum_{\Delta \in \Gamma_\Delta} \mathbb{E} [\mathcal{C}^I(\Delta)]^2}{\frac{1}{|\Gamma_\Delta^c|} \sum_{\Delta \in \Gamma_\Delta^c} \text{Var} [\mathcal{C}^I(\Delta)]} \quad (9)$$

One way to increase the correlation contrast used by [1], is to capture multiple images of the latent pattern O behind different scattering layers. Effectively, we measure $I_t = S_t^0 \star O$ with different speckle patterns S_t^0 . The auto-correlation is then evaluated as the average of the individual auto-correlations

$$\mathcal{C}^{\bar{I}_1, \dots, \bar{I}_T}(\Delta) = \frac{1}{T} \sum_t \mathcal{C}^{\bar{I}_t}(\Delta), \quad (10)$$

with $\mathcal{C}^{\bar{I}_t} = \bar{I}_t \star \bar{I}_t$ as defined in Eq. (8).

In supplement Sec. A, we formally prove the following.

Claim 1 *If the speckle patterns S_t^0 are uncorrelated with each other for different t values, then replacing \mathcal{C}^I with $\mathcal{C}^{\bar{I}_1, \dots, \bar{I}_T}$ in the correlation contrast of Eq. (9) increases the contrast linearly with the number of measurements T , i.e.,*

$$\Theta(\mathcal{C}^{\bar{I}_1, \dots, \bar{I}_T}) = T \cdot \Theta(\mathcal{C}^I). \quad (11)$$

While this is a promising idea, when the sources are located inside the tissue, it is not easy to image the same illuminators through different scattering layers. Rather, in this work, we would like to modify the speckle patterns by adjusting the optics.

Random modulation. Intuitively, to create different speckle intensity images, we can put a random phase mask in the optical path between the sample to the imaging sensor. If we put this mask in the Fourier plane, it would translate into a convolution of the fields $u^i(\mathbf{v})$ with the Fourier transform of the mask, which we denote as h_t . This would lead into an intensity image $I_t = \sum_n S_t^n$ with

$$S_t^n = |u^n \star h_t|^2. \quad (12)$$

In Fig. 2(c), we compare the auto-correlation of a single speckle image to the average auto-correlation with 54 random masks h_t . Averaging random masks rejects noise and improves the correlation contrast, but it is still noisy.

To understand why random modulation is sub-optimal, we review the tilt-shift correlation in Eq. (1). If the fields u^1, u^2 generated by different illuminators would follow a pure shift, then $u^1 \star h_t, u^2 \star h_t$ would also be shifted versions of each other. However, according to Eq. (1), fields from different sources vary by phase, and hence a convolution with h_t largely degrades the correlation and $S_t^1(\mathbf{v})$ would differ from $S_t^2(\mathbf{v} + \Delta)$.

Lateral Shearing Interferometry. Our goal in this work is to change the optical path such that we can capture multiple uncorrelated speckle patterns, and yet maintain the ME correlation. To this end, we build a lateral shearing interferometry (LSI) [23] setup that allows us to measure the interference between u^{i^n} and a shifted copy of it. This leads to a measurement of the form

$$S_t^{i^n} = u^{i^n}(\mathbf{v})u^{i^n}(\mathbf{v} + \mathbf{d}_t)^*, \quad (13)$$

where \mathbf{d}_t denotes the displacement vector. We acquire these measurements using an incoherent interferometry scheme along the lines of FINCH [24, 25], described in Sec. 3.C. The set of displacements used in our implementation is described and visualized in supplement Sec. D.

When several incoherent sources are present, we will acquire an incoherent summation

$$I_t = \sum_n S_t^{i^n}. \quad (14)$$

This interferometric measurement is already a zero mean signal and there is no need to subtract the mean as with the intensity measurements of Eq. (4).

The LSI measurements provide two main benefits which we summarize in the following claims and prove in supplement Sec. A. First, unlike a naive optical mask in Eq. (12), it does not reduce the ME correlation of the original speckles. Second, despite the fact that these measurements are captured from the same tissue layer and they are not independent, they are still *uncorrelated*.

Claim 2 *For displacements in the order of a few speckle grains, the correlation between LSI signals $S_t^{i^1}, S_t^{i^2}$ produced by different illuminators i^1, i^2 is approximately the same as the correlation of the original speckle intensity images.*

Claim 3 *For displacements $\mathbf{d}_{t_1}, \mathbf{d}_{t_2}$ whose distance $\|\mathbf{d}_{t_1} - \mathbf{d}_{t_2}\|$ is larger than the speckle grain, the signals $S_{t_1}^{i^n}, S_{t_2}^{i^n}$ are uncorrelated.*

The observation in Claim 3 is central to this paper. The fact that different displacements lead to uncorrelated speckle measurements means that according to Claim 1, we could average them and the auto-correlation contrast would improve *linearly* with the number of measurements.

The auto-correlation of the LSI measurements relates to the auto-correlation of the hidden illuminator pattern O , but unlike pure intensity speckles, with the above modulations a phase correction is needed, which we derive in the following claim, and prove in supplement Sec. A.

Claim 4 *Using the LSI measurements of Eq. (13), the speckle auto-correlation $\mathcal{C}^{I_t} = I_t \star I_t$ approximates the auto-correlation of the latent pattern $\mathcal{C}^O = O \star O$, times a phase ramp correction*

$$\mathcal{C}^{I_t}(\Delta) \approx e^{-jk\alpha(\mathbf{d}_t^T \Delta)} \mathcal{C}^O(\Delta). \quad (15)$$

Given the relation in Claim 4, we average the auto-correlation of the different LSI measurements, applying the phase ramp correction of Eq. (15):

$$\mathcal{C}^{I_1, \dots, I_T} = \frac{1}{T} \sum_t e^{jk\alpha(\mathbf{d}_t^T \Delta)} \mathcal{C}^{I_t}(\Delta) \quad (16)$$

The phase corrected averaging in Eq. (16) is subject to a single unknown parameter α . α can be driven from ME theory based on knowledge of the tissue thickness [21], but in our implementation, we manually tune it to maximize the visual quality of the results, as discussed in supplement Sec. F.

Visualizing averaged correlations. In Fig. 2(d) we show the auto-correlation obtained by averaging LSI measurements I_t (Eq. (14)) with the phase ramp correction of Eq. (16). Our approach reduces noise and improves the correlation contrast when compared with random modulations (Eq. (12)) or just with the auto-correlation of a single speckle image.

In Fig. 2(d), we average 18 LSI measurements I_t . Note that as we explain in Sec. 3.C capturing each interferometric measurement I_t requires 3 shots, so the 18 measurements in Fig. 2(d-e) are acquired using a total of 54 shots. This is compared against 54 independent measurements captured by the random modulation approach. The 18 LSI modulations are superior to the 54 random modulations.

We note that the LSI measurements used here are similar to those used in wavefront sensing [23]. However, one usually uses smaller displacements in wavefront sensing to obtain the local gradient of the wave, while the displacements we use here are larger than the speckle grain size so that we obtain uncorrelated speckles.

C. Exploiting local support

The previous section aims at increasing the auto-correlation contrast by averaging multiple measurements. To improve on it, we adopt a recent approach by Alterman *et al.* [11]. This allows us to recover target patterns which are larger than the extent of ME correlations, as well as complementary noise reduction.

The approach is based on the observation that when the light sources are inside the sample, rather than far behind it, the speckle pattern scattered from a single source has *local support*, *i.e.*, the scattered light does not spread over the entire sensor. Therefore, it is argued that computing the full-frame auto-correlation over the entire image corrupts the signal with additional noise. Rather, it is sufficient to match the local correlations of the observed speckle pattern and the optimized latent image. This leads into a Ptychography style cost [26]. We review the exact cost in supplement Sec. B. In the experimental section below, we show that moving from full-frame correlations to local ones has a major impact on noise elimination and improving the resulting reconstruction.

Another advantage of the local cost discussed in [11], is that it allows recovering patterns larger than the extent of the ME. As mentioned above, ME correlations of the form of Eq. (1) only hold for small displacements Δ . When matching the full-frame auto-correlation (Eq. (6)) of I and O , we rely on the fact that ME correlation exists between any two sources in our latent pattern. This assumption largely limits the range of recoverable illuminator patterns to patterns lying within the ME range. In contrast, the local cost only relies on local correlations between sources in the same local window. At the same time, the overall extent of the illuminator pattern O can be larger than these local windows.

Algorithm summary. Our approach is summarized in Fig. 3. Given a fluorescent target we capture a set of diversified speckle patterns. We calculate the local auto-correlation in all sub-windows of each diversified pattern. We then average all the diversified auto-correlations of each sub-window, resulting in a cleaner local auto-correlation and a higher SNR contrast. Finally we solve for a latent pattern whose local auto-correlations best agree with the measured ones.

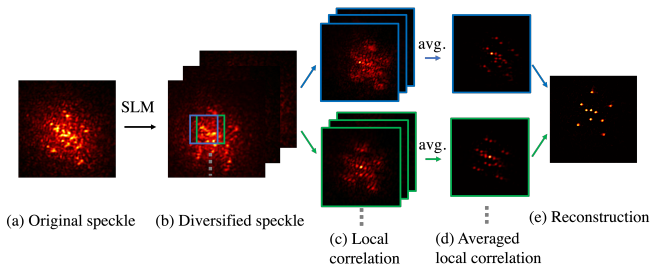


Fig. 3. Flow chart. (a) The original speckle. (b) Our approach captures multiple diversified speckle images of the same target, rather than a single image. (c) In each sub-window of the frame we calculate the local auto-correlations of all diversified speckle images. (d) By averaging the local auto-correlations from multiple speckles we can largely improve their SNR. (e) We reconstruct the target following the approach of [11], searching for a latent pattern that jointly explains all local correlations.

3. ACQUISITION

The results in this paper were captured using two complementary setups. A fluorescent imaging setup described in Fig. 4 and a secondary setup allowing us to program incoherent layouts for accessible analysis, described in Fig. 5.

A. Main fluorescent imaging setup

Fig. 4 illustrates our acquisition setup, including an imaging arm and a validation arm. The imaging arm consists of an objective and a tube lens, followed by a second relay system which allows us to place a spatial light modulator (SLM) at the Fourier plane. The image of the modulated field is collected by the main camera. The objective attempts to image fluorescent sources beyond a scattering sample. A second validation camera images the beads from the other end of the tissue, allowing the capture of a clear unscattered image of the illuminator layout, which is used to assess reconstruction quality. Note that this validation camera does not provide any input to the algorithm. The target and the validation objectives are mounted on z-axis translation stages, facilitating accurate control over focusing in both imaging and validation arms.

For most of our experiments, we used chicken breast tissue as a scattering sample. In the supplement, we also demonstrate results imaging through a parafilm tissue phantom. We discuss what is known about the optical characterization of these materials in supplement Sec. H. We used Spherotech Fluorescent Nile Red Particles $0.4 - 0.6\mu\text{m}$, FP-0556-2. The beads are attached on a microscope cover glass behind the scattering tissue. The separation between the beads and the tissue is as low as $150\mu\text{m}$, the thickness of the cover glass. The beads are excited with a 530nm laser from the front side of the tissue. The excitation light scatters through the tissue, illuminates the beads, and the emitted light scatters back through the tissue to the camera. We filtered the excited light using a 10nm bandpass filter centered at 580nm .

B. Analysis setup for programmable incoherent targets

We wanted to test our algorithm on incoherent illumination layout of arbitrary complexity. Thus, in addition to fluorescent beads we created incoherent illumination patterns with a translating laser using the setup illustrated in Fig. 5. For this, we

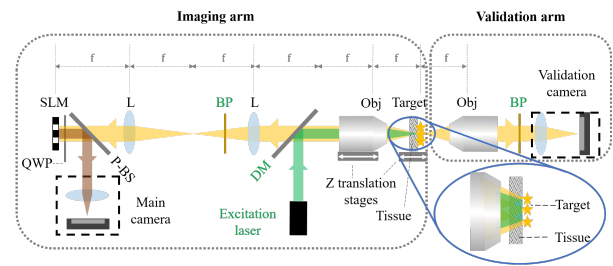


Fig. 4. Experimental setup. We attach fluorescent beads at the back of a tissue layer. A laser excites the beads from the front side of the tissue. The emitted light is back scattered through the tissue and collected by the main camera. We create a $4f$ relay system in the optical path and place an SLM in its Fourier plane to modulate the scattered light. Finally, we used a validation camera behind the tissue which can image the beads directly. This camera is not part of our algorithm and is only used to validate its output. L: lens. Obj: objective lens. BP: bandpass filter. QWP: quarter wave plate. P-BS: polarized beam splitter. DM: dichromatic mirror.

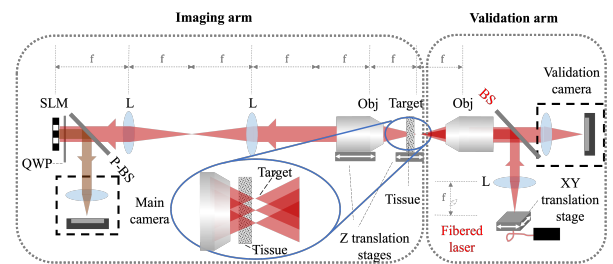


Fig. 5. Alternative experimental setup. For analysis propose we also synthesis incoherent latent patterns using a translating laser. The diffused output of a fibered laser is imaged using a tube lens and objective to generate a diffused source exactly at the back plane of a tissue layer. The laser light is scattered through the tissue and the speckle pattern it generates is imaged by the main camera from the other side of the tissue. We mount a fibered laser on a 2D translation stage so we can create programmable patterns. The intensity images captured at multiple source positions are summed to simulate an incoherent image.

imaged the diffused output of a fibered laser (635nm) to generate a point focused exactly at the back of the tissue (we use the validation camera for accurate focusing). The main camera at the other side of the tissue captured the intensity scattered from this spot. We then translate the fiber output on a programmable xy stage to generate spots at other positions behind the tissue. We capture a sequence of images at each source position and sum their intensities, thus simulating incoherent summation from multiple sources. This setup allows us to control the layout and complexity of the sources, which is useful for analyzing our algorithm with patterns of controlled complexities.

Throughout the experimental section, we visualize images of fluorescent beads with a green colormap, and translating laser images with a red colormap.

C. Interferometric measurements

To capture our diversified speckles we borrow ideas from Fresnel incoherent correlation holography (FINCH) [24, 25]. While most of our setup is similar to the one used by [11], we use an SLM (Holoeye LETO) in the Fourier plane of the imaging arm, which we use to modulate the scattered light. To capture interferometric measurements, we use a polarizing beamsplitter to horizontally polarize the wave, followed by a quarter waveplate at an angle of 45° to induce a $\pi/2$ phase delay along one of the axis to produce a circularly polarized light. The SLM only modulates the polarization state along its fast axis, which is horizontal, and its slow axis is reflected without any modulation. The light reflected off the SLM is sent again through quarter waveplate, which adds another $\pi/2$ phase shift that makes the light linearly polarized again, but in a vertical direction; finally, the polarizing beamsplitter interferes the modulated and unmodulated waves. To capture the LSI measurements of Eq. (13), we place on the SLM a phase ramp whose frequency and orientation matches the translation \mathbf{d}_t we want to implement. We capture $K = 3$ images of this phase ramp plus a global phasor $\phi_k \in \{0, \frac{\pi}{3}, \frac{2\pi}{3}\}$. Since the SLM modulates only part of the wave, we obtain the measurement

$$\hat{S}_t^{i^n, k} = \left| u^{i^n}(\mathbf{v}) + e^{j\phi_k} u^{i^n}(\mathbf{v} + \mathbf{d}_t) \right|^2, \quad (17)$$

where k index the phase shift, n index the fluorescent source, and t index the translation \mathbf{d}_t of the current measurement. Using phase-shifting interferometry [27], we can extract the interference signal desired in Eq. (13) as:

$$S_t^{i^n} = \sum_k e^{j\phi_k} \left| u^{i^n}(\mathbf{v}) + e^{j\phi_k} u^{i^n}(\mathbf{v} + \mathbf{d}_t) \right|^2 = u^{i^n}(\mathbf{v}) u^{i^n}(\mathbf{v} + \mathbf{d}_t)^*, \quad (18)$$

In the presence of multiple incoherent sources, emission from different sources do not interfere. Thus, the measured intensity in each shot is equivalent to $\hat{I}_t^k = \sum_n \hat{S}_t^{i^n, k}$. With the phase shifting interferometry in Eq. (18) we extract $I_t = \sum_n S_t^{i^n}$.

Throughout this work we used 18 \mathbf{d}_t displacements described in supplement Sec. D. Since each interferometric measurement uses 3 images, this requires a total of 54 shots.

4. RESULTS

A. Experiment results

We start by demonstrating our setup on a fluorescent bead target. In Fig. 1, we reconstruct a 1000×1000 pixel image, corresponding to a field of view of $300\mu m \times 300\mu m$. The random beads were spread behind a $\sim 150\mu m$ thick tissue. Note that all thickness measurements in this paper are approximated due to the limited resolution of the clipper. The bead layout is unrecognizable from the captured speckle input. Moreover, as so many independent incoherent sources are present, the input images are rather smooth and speckle variation is almost invisible. Despite this, our LSI framework achieves a clear reconstruction from 54 shots. Additional results are included in Supplement Fig. S7 and S14.

While the reference and the reconstruction have the same layout they have somewhat different brightness and resolution. The resolution of the reference is subject to the diffraction limit. The reconstruction algorithm on the other hand encourages sparse results, and hence, recovered dots tend to be narrower. The brightness variation is partially attributed to the fact that the reference is captured by a different camera from a different direction, but also due to imperfect convergence of our optimization.

B. Comparing reconstruction and diversification approaches

In Fig. 6, we evaluate two components of our algorithm: (i) the usage of local correlations [11] discussed in Sec. 2.C, versus the standard full frame auto-correlation used in previous work [1, 2, 10], and (ii) the diversification approach.

As discussed in [11] and reviewed in Sec. 2.C, the local approach detects correlations with a higher SNR compared to the full frame approach and indeed it leads to better reconstructions. We also show that the LSI leads to better results compared to simpler diversification alternatives.

Fig. 6 compares different diversification schemes, as well as evaluates the effectiveness of full-frame and local-correlation algorithms. The top row of the figure shows reconstructions of a spatially-incoherent target with a simple structure. For the full frame approach, a single shot results in unrecognizable reconstruction, that is only slightly improved given 54 random modulations. In contrast, our LSI approach can correctly reconstruct the pattern. The usage of local correlations compared to full-frame ones reduces some of the noise, and hence even random modulations can lead to good reconstruction.

The bottom row of the figure compares reconstructions on a denser fluorescent bead target. As explained in [11], the increased source density is more challenging to reconstruct as the contrast of the incoherent speckle image decreases. The full-frame approach fails to reconstruct this target with any of the diversification approaches. The local correlation algorithm fails with a single shot (no diversification). The random modulation reconstructed only a subset of the beads, and the best results are obtained using LSI approach.

The patterns recovered in Fig. 6 have a small extent. We note however, that for wide patterns the local approach of [11] has another important advantage, as it can reconstruct patterns wider than the range of ME correlation.

C. Structured targets

Fig. 7 demonstrates reconstruction of structured patterns using the translating laser setup rather than sparse beads. As this setup allows us to program the layout of the latent sources we can test the reconstruction of structured targets. At the top row we have generated a star shape target, so that sources density varies between the center and periphery. As predicted by theory, reconstruction from a single image can only recover the periphery of the pattern where illuminators are sparse. Our LSI can handle higher source density and can recover a larger part of the star, only facing a small difficulty at the very center.

In the second row of Fig. 7 we reconstruct a wide structured pattern. As we had access to the speckles produced by each source independently, we could also compute the extent of the memory effect, plotted in supplement Fig. S12. The pattern we have recovered is significantly wider than the range at which ME correlation is present. This property was exhaustively demonstrated by [11], and we refer the reader to their article for further details.

D. Contrast improvement for different diversifications

Below we test the improvement in correlation contrast as well as the reconstruction results as a function of the number of diversification measurements.

In Fig. 8 we plot the correlation contrast of Eq. (9) as a function of the number of averaged images T . We start by capturing multiple images without any diversification. This only reduces

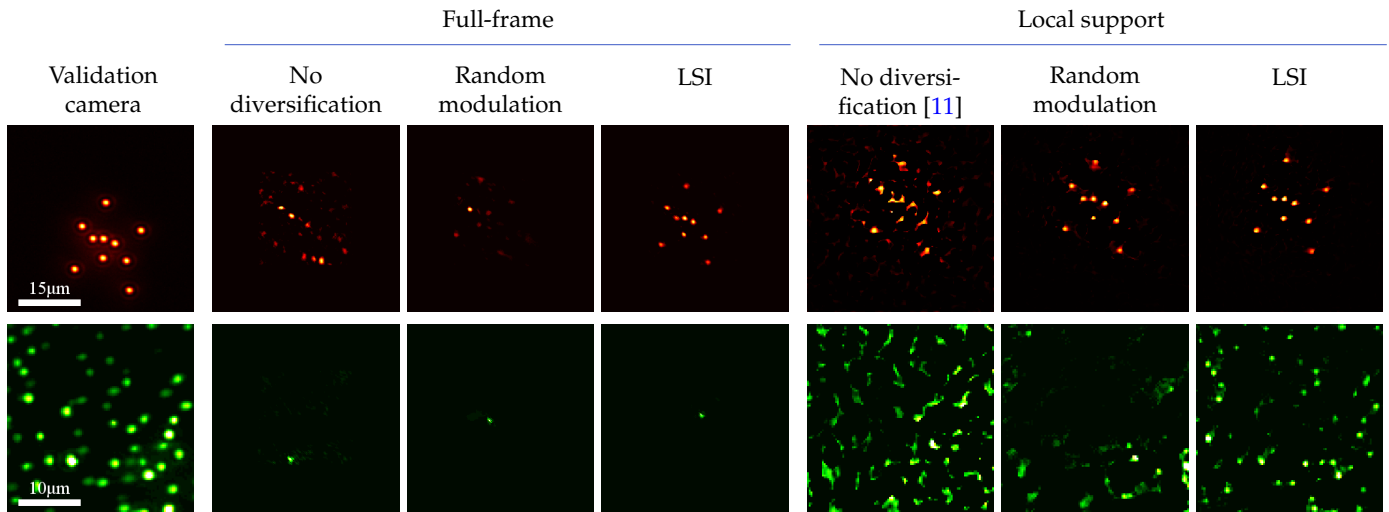


Fig. 6. Comparing reconstruction and modulation approaches. Top part: a spatially incoherent target with a sparse and simple layout. Lower part: challenging fluorescent beads target. Local support correlations [11] are stronger than standard full-frame auto-correlations [10], and our LSI improves over a single shot (with no diversification) and over simple random modulation. For the simple target on the top, the full-frame algorithm can recover the image given the improved correlation provided by LSI modulations, but fails to do so from the noisier correlations provided by other diversification strategies. The local correlation approach which is more robust to noise can recover the target even with the simpler modulations. For the challenging target at the lower part, the full-frame algorithm fails completely using all types of diversification. The local correlations algorithm can reconstruct the target using LSI modulations. However given random modulations, it can only reconstruct a subset of the beads.

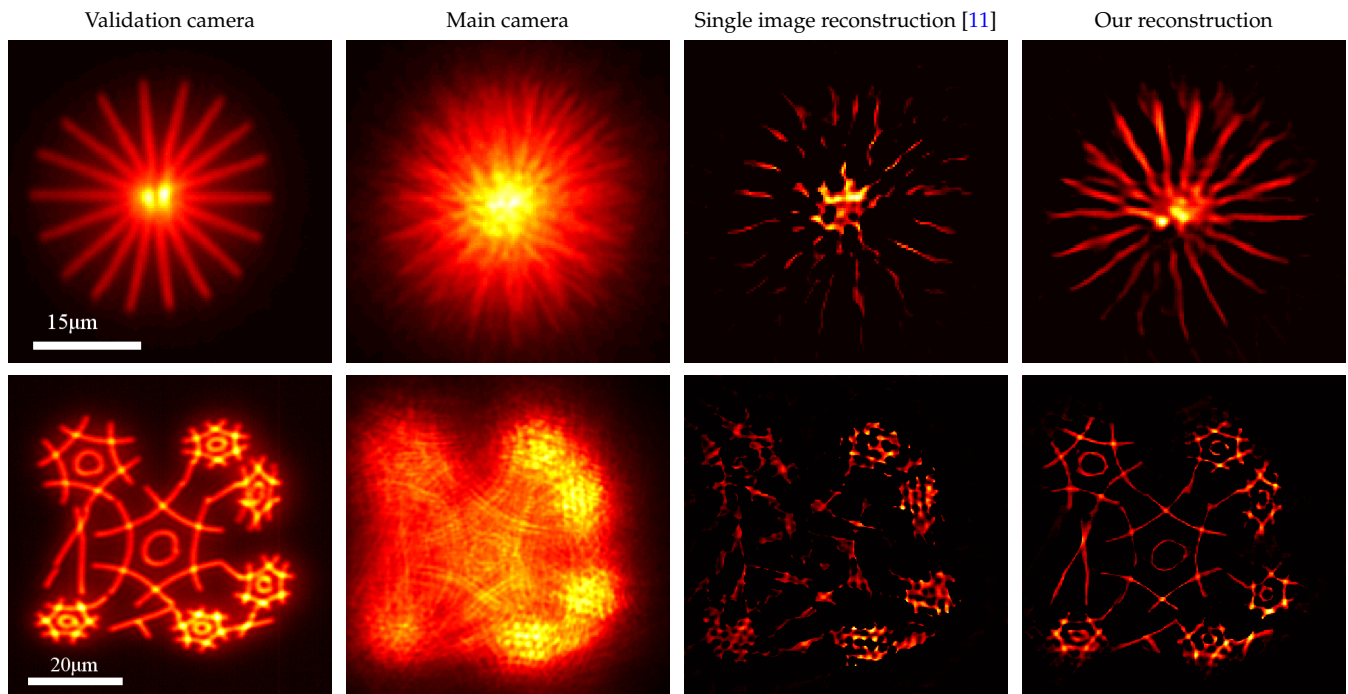


Fig. 7. Reconstruction results from a spatially incoherent target. We reconstruct two spatially incoherent targets with more complicated layouts behind $\sim 150\mu\text{m}$ -thick tissue slice.

read and photon noise, which does not translate into a real improvement in correlation contrast. When we randomly modulate the wave (Eq. (12)), the contrast increases but it eventually saturates as the convolution reduces the ME correlation. By using our LSI (Eq. (13)), the contrast increases roughly linearly as pre-

dicted by the theory. This suggests that the speckle signals S_t we generate are indeed uncorrelated for different displacements $\mathbf{d}_{t_1}, \mathbf{d}_{t_2}$. The graphs in Fig. 8 demonstrate correlation contrast observed with two different tissue slices. For each of the tissue slices, we generated the source layout in the top row of Fig. 2.

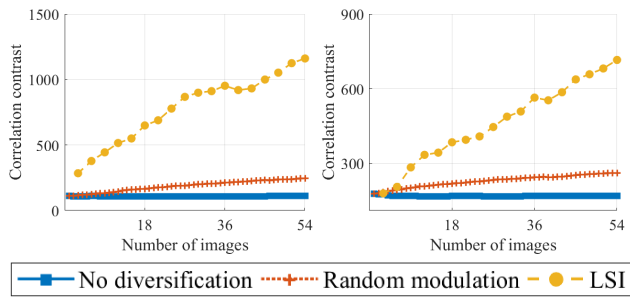


Fig. 8. Contrast improvement for different diversification. We compare speckle correlation contrast as a function of the number of images for different modulation approaches. The two images show correlation contrast measurements for two different tissue slices. The graphs are noisy due to the finite speckle spread in an image, but still demonstrate clear differences between different diversification approaches. Without diversification, multiple images only reduce read and photon noise of the image, which does not lead to a significant improvement in contrast. Multiple images with random modulations can improve contrast, but the gain saturates quickly as ME degrades. On the other hand, LSI can achieve a higher contrast, and, in agreement with theory, contrast increases roughly linearly with the number of shots.

As we evaluate speckles through real tissue, we note that: 1) the exact amount of correlation we measure in each tissue slice can vary, and 2) each tissue layer generates a speckle spread with a limited support. As we only average a finite number of speckle pixels, the graphs are noisy. Despite these issues, the graphs measured from difference slices demonstrate consistent trends.

In Fig. 9, we visually compare reconstructions using an increasing number of input images, and demonstrate how the improved contrast translates into better reconstruction quality. This experiment uses the same bead layout as in the lower part of Fig. 6, please refer to the validation camera reference displayed there. In supplement Sec. D, we further show that the results are rather insensitive to the exact selection of displacements \mathbf{d}_i .

5. DISCUSSION

In this work, we demonstrate the reconstruction of fluorescent illuminator patterns attached to a scattering tissue. Despite scattering that completely distort the captured images, we can exploit ME correlations in the measured speckles to detect the hidden illuminator layout. While such correlations are inherently weak, we suggest a diversification scheme which allows us to capture multiple uncorrelated speckle measurements of the same sources. By averaging the correlations of such measurements, we increase the signal to noise ratio in the data and largely boost the reconstruction quality. We combine these modulated measurements with a recent algorithm [11] seeking a latent pattern whose local correlations agree with local correlations in the measured data. The local correlations provide additional improvement in SNR. Moreover, since it only assumes local correlations between the speckles emitted by nearby sources rather than global full-frame correlations between any two sources in the image, it allows us to reconstruct wide patterns, much beyond the limited extent of the ME. Overall, we demonstrate the reconstruction of mega-pixel wide patterns, limited only by the sensor size.

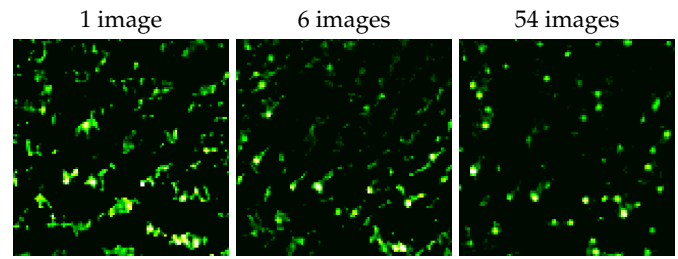


Fig. 9. Evaluating reconstruction vs. number of shots. We visualize the quality of the reconstruction given no modulation (single shot), and with an increasing number of modulation patterns. As evaluated numerically in Fig. 8 the correlation contrast increases linearly with the number of shots and in agreement, the visual quality of the reconstruction improves. The reference speckle layout in this experiment is equivalent to the validation camera image in the lower part of Fig. 6.

The lateral resolution of our approach is set by the NA of the imaging optics. At the same time we have only studied the reconstruction of planar targets and extending the approach to recover 3D targets is left for future research.

Despite the advances offered by this approach, it is inherently dependent on the existence of some ME correlation; thus when such correlations are too weak to be measured, our approach will fail as well. Two major factors that decrease the ME correlations are the tissue thickness and the number of independent incoherent sources. In our current implementation, we recovered sources behind $150\mu\text{m}$ -thick tissue, which is beyond the penetration depth of a standard microscope. While this significantly advances the capabilities of a standard microscope, numerous biomedical applications would benefit from increasing this depth further. The second challenge for ME-based correlations is that we assume speckle variation is observed in the captured data. As more and more independent sources are present, the speckle contrast decays and the captured intensity images are smoother. Naturally, when speckle contrast is lower than the photon noise in the data, no correlations can be detected. Hence ME-based techniques are inherently limited to simple, sparse illuminator layouts.

An alternative approach for seeing through scattering tissue is based on wavefront shaping optics. Rather than post-process the speckle data, it attempts to modulate the incoming excitation light and/or the outgoing emission, to undo the tissue aberration in optics. In theory, this approach carries the potential to extend to thicker tissue layers and to correct complex patterns. In practice, efficiently finding a proper modulation mask is a challenging task. Recently, [20] has managed to recover such a modulation efficiently using linear (single photon) fluorescent feedback from a sparse set of beads. However, even after recovering a good modulation mask, the area they could correct with it is limited due to the limited extent of the ME. In contrast, our approach can recover wide-field-of-view, full-frame images, as it only relies on local ME correlations.

Acknowledgments. We thank Lucia Lu for preparing fluorescent samples.

Disclosures. The authors declare no conflicts of interest.

Data Availability. Data and code underlying the results presented in this paper are available in <https://github.com/Image-Science-Lab-cmu/EnhancingSpeckle>

Supplemental document. See Supplement 1 for supporting content.

REFERENCES

- O. Katz, P. Heidmann, M. Fink, and S. Gigan, "Non-invasive single-shot imaging through scattering layers and around corners via speckle correlation," *Nat. Photonics* (2014).
- J. Bertolotti, E. G. van Putten, C. Blum, A. Lagendijk, W. L. Vos, and A. P. Mosk, "Non-invasive imaging through opaque scattering layers," (2012).
- K. T. Takasaki and J. W. Fleischer, "Phase-space measurement for depth-resolved memory-effect imaging," *Opt. Express* (2014).
- E. Edrei and G. Scarcelli, "Optical imaging through dynamic turbid media using the fourier-domain shower-curtain effect," *Optica* (2016).
- E. Edrei and G. Scarcelli, "Memory-effect based deconvolution microscopy for super-resolution imaging through scattering media," *Sci. Reports* (2016).
- M. Hofer, C. Soeller, S. Brasselet, and J. Bertolotti, "Wide field fluorescence epi-microscopy behind a scattering medium enabled by speckle correlations," *Opt. Express* (2018).
- T. Wu, J. Dong, X. Shao, and S. Gigan, "Imaging through a thin scattering layer and jointly retrieving the point-spread-function using phase-diversity," *Opt. Express* (2017).
- T. Wu, J. Dong, and S. Gigan, "Non-invasive single-shot recovery of a point-spread function of a memory effect based scattering imaging system," *Opt. Lett.* (2020).
- X. Wang, X. Jin, and J. Li, "Blind position detection for large field-of-view scattering imaging," *Photon. Res.* (2020).
- J. Chang and G. Wetzstein, "Single-shot speckle correlation fluorescence microscopy in thick scattering tissue with image reconstruction priors," *J. Biophotonics* (2018).
- M. Alterman, C. Bar, I. Gkioulekas, and A. Levin, "Imaging with local speckle intensity correlations: theory and practice," *ACM TOG* (2021).
- M. Zhou, A. Pan, R. Li, Y. Liang, J. Min, T. Peng, C. Bai, and B. Yao, "Retrieval of non-sparse object through scattering media beyond the memory effect," *J. Opt.* (2020).
- D. F. Gardner, S. Divitt, and A. T. Watnik, "Ptychographic imaging of incoherently illuminated extended objects using speckle correlations," *Appl. Opt.* (2019).
- G. Li, Y. Wanqin, W. Haichao, and G. Situ, "Image transmission through scattering media using ptychographic iterative engine," *Appl. Sci.* (2019).
- L. Li, X. Wen, R. Song, J.-T. Jiang, H.-L. Zhang, X.-B. Liu, and L. Wei, "Imaging correlography using ptychography," *Appl. Sci.* (2019).
- N. Shekel and O. Katz, "Using fiber-bending-generated speckles for improved working distance and background rejection in lensless microendoscopy," *Opt. Lett.* **45**, 4288–4291 (2020).
- A. Boniface, J. Dong, and S. Gigan, "Non-invasive focusing and imaging in scattering media with a fluorescence-based transmission matrix," *Nat. Commun.* (2020).
- L. Zhu, F. Soldevila, C. Moretti, A. d'Arco, A. Boniface, X. Shao, H. B. de Aguiar, and S. Gigan, "Large field-of-view non-invasive imaging through scattering layers using fluctuating random illumination," *arXiv preprint arXiv:2017.08158* (2021).
- A. Boniface, B. Blochet, J. Dong, and S. Gigan, "Noninvasive light focusing in scattering media using speckle variance optimization," *Optica* (2019).
- D. Aizik, I. Gkioulekas, and A. Levin, "Fluorescent wavefront shaping using incoherent iterative phase conjugation," *arXiv preprint* (2022).
- G. Osnabrugge, R. Horstmeyer, I. N. Papadopoulos, B. Judkewitz, and I. M. Vellekoop, "Generalized optical memory effect," *Optica* (2017).
- C. Bar, M. Alterman, I. Gkioulekas, and A. Levin, "Single scattering modeling of speckle correlation," in *ICCP*, (2021).
- M. Riley and M. Gusinow, "Laser beam divergence utilizing a lateral shearing interferometer," *Appl. Opt.* **16**, 2753–2756 (1977).
- J. Rosen and G. Brooker, "Fresnel incoherent correlation holography (finch): a review of research," *Adv. Opt. Technol.* **1**, 151–169 (2012).
- J. Rosen, S. Alford, V. Anand, J. Art, P. Bouchal, Z. Bouchal, M.-U. Erdenebat, L. Huang, A. Ishii, S. Juodkazis *et al.*, "Roadmap on recent progress in finch technology," *J. Imaging* **7**, 197 (2021).
- J. M. Rodenburg, A. C. Hurst, A. G. Cullis, B. R. Dobson, F. Pfeiffer, O. Bunk, C. David, K. Jefimovs, and I. Johnson, "Hard-x-ray lensless imaging of extended objects," *Phys. Rev. Lett.* **98** (2007).
- P. Hariharan, B. Oreb, and T. Eiju, "Digital phase-shifting interferometry: a simple error-compensating phase calculation algorithm," *Appl. Opt.* **26**, 2504–2506 (1987).